China Geology 7 (2024) 222–236

China Geology

Journal homepage: http://chinageology.cgs.cn
https://www.sciencedirect.com/journal/china-geology

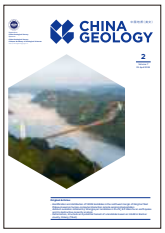

Dynamic simulation insights into friction weakening effect on rapid long-runout landslides: A case study of the Yigong landslide in the Tibetan Plateau, China

Zi-zheng Guo[a], Xin-yong Zhou[a], Da Huang[b,*], Shi-jie Zhai[a], Bi-xia Tian[a], Guang-ming Li[c]

[a] *School of Civil and Transportation Engineering*, *Hebei University of Technology*, *Tianjin* 300401, *China*
[b] *School of Geological Engineering and Geomatics*, *Chang'an University*, *Xi'an* 710054, *China*
[c] *Tianjin Municipal Engineering Design & Research Institute (TMEDI)*, *Tianjin* 300392, *China*

ARTICLE INFO

Article history:
Received 13 January 2024
Received in revised form 21 March 2024
Accepted 25 March 2024
Available online 10 April 2024

Keywords:
Rapid long-runout landslide
PFC
Friction weakening
Three-dimension
Numerical simulation
Tibetan Plateau
Hydrogeology Engineering
Geological hazards survey engineering

ABSTRACT

This study proposed a novel friction law dependent on velocity, displacement and normal stress for kinematic analysis of runout process of rapid landslides. The well-known Yigong landslide occurring in the Tibetan Plateau of China was employed as the case, and the derived dynamic friction formula was included into the numerical simulation based on Particle Flow Code. Results showed that the friction decreased quickly from 0.64 (the peak) to 0.1 (the stead value) during the 5s-period after the sliding initiation, which explained the behavior of rapid movement of the landslide. The monitored balls set at different sections of the mass showed similar variation characteristics regarding the velocity, namely evident increase at the initial phase of the movement, followed by a fluctuation phase and then a stopping one. The peak velocity was more than 100 m/s and most particles had low velocities at 300s after the landslide initiation. The spreading distance of the landslide was calculated at the two-dimension (profile) and three-dimension scale, respectively. Compared with the simulation result without considering friction weakening effect, our results indicated a max distance of about 10 km from the initial unstable position, which fit better with the actual situation.

1. Introduction

As the region with the highest average altitude in the world, the Tibetan Plateau is formed by the compression and uplift of the tectonic plates (Royden LH et al., 2008). In recent years, a large amount of geohazards induced by excessive infiltration in the forms of rainfall and ice or snow melting were reported in the area. A quite large proportion of them were rapid long-runout landslides (Fort M, 2000; Schneider D et al., 2011; Zhang M and Yin Y, 2013; Guo Z et al., 2023), which have resulted in considerable injuries and economic losses (Xing A et al, 2015; Qi W et al., 2021). Therefore, accurately predicting the kinematic process is key to reducing the risk for such catastrophic landslides.

Rapid long-runout landslides commonly have broader threating ranges and more significant consequences compared with slow-moving landslides (Dawso AG et al., 2017; Guo Z et al., 2020a). Currently, numerous methods have been developed and employed for dynamic simulation and assessment of rapid long-runout landslides, such as the rapid mass movement simulation (Huang T et al., 2017), the depth-integrated continuum method (Ouyang C et al., 2017), and the depth-averaged model (Liu W and He S, 2018). Furthermore, many numerical simulation software have been also applied to evaluate the movement and impact areas of rapid long-runout landslides, including DAN, PFC (Wei J et al., 2019), DDA (Song Y et al., 2016), UDEC (Luo J et al., 2019), SPH (Zhu C et al., 2018), and their coupling methods (Zhao T et al., 2017, Wang W et al., 2016). However, most studies only involved two-dimensional scale (Pritchard MA and Savigny K, 1991, Zhang Z et al., 2017), which didn't completely reflect the topographic and geomorphic conditions in which the landslides occurred. The primary reasons for this issue are associated with data availability, the complexity of three-dimensional modeling, and similar factors (Jaboyedoff M et al., 2012). Certainly, actual contexts of the case and the applicable conditions of numerical models are also the

First author: *E-mail address*: zizheng.guo@hebut.edu.cn (Zi-zheng Guo).

* Corresponding author: *E-mail address*: huangda@chd.edu.cn (Da Huang).

Literary editor: Xi-jie Chen
doi:10.31035/cg2023132
2096-5192/© 2024 China Geology Editorial Office.

constraints. Hence, users should select the modelling approach according to the results that they attend to present. Although some methods for three-dimensional modeling of geological bodies have been developed (Wu JH et al., 2018), more case studies of rapid long-runout landslides worldwide are still needed to provide the latest insights on this topic.

As is well-known, landslides typically undergo a change in friction from increasing to decreasing from initiation to completion, and the variation in the friction coefficient is closely related to the movement process (Zhang H et al., 2023). However, many studies have overlooked this aspect. For example, Feng ZY et al. (2017) used a PFC-FLAC coupled method to simulate the Xiaolin landslide in Taiwan of China, but analyzed the friction coefficient as a constant value. Currently, research on friction forces during landslide movement mainly involves theoretical analysis (Zhao T et al., 2020), field investigations (Lin A et al., 2010), laboratory experiments (Mizoguchi K et al., 2007; Ma P et al., 2022), and numerical simulations (Liu W et al., 2016). For instance, Moore DE and Lockner DA (2008) confirmed from the perspective of the conversion of friction to thermal energy that saturated rock blocks had low friction during the movement. Song Y et al. (2016) based on the relationship between friction and velocity-displacement, used DDA to simulate the Daguangbao landslide in Sichuan of China. Wang Y et al. (2017; 2018) conducted high-velocity rotary shear experiments on the soil sample of the Yigong landslide and observed a noticeable friction weakening dependent on velocity and normal stress characteristics. However, these studies typically analyzed the influence of single or two factors on friction and could not comprehensively consider the combined effects of displacement, velocity, and normal stress. This can lead to biases in simulating frictional weakening phenomena in rapid long-runout landslides.

The main objective of the present study is to perform dynamic simulation of rapid long-runout landslide through considering the effect of friction weakening. Specifically, our aims include: (i) the derivation of the relationship among the friction with velocity, displacement and normal stress, (ii) the determination of the dynamic friction formula of the Yigong landslide in China through the shear test results, and (iii) the numerical simulation of the Yigong landslide considering the friction weakening effect to assess the dynamic runout process.

2. Geological backgrounds

2.1. Basic characteristics of the Yigong landslide

On April 9, 2000, the Yigong landslide occurred in the

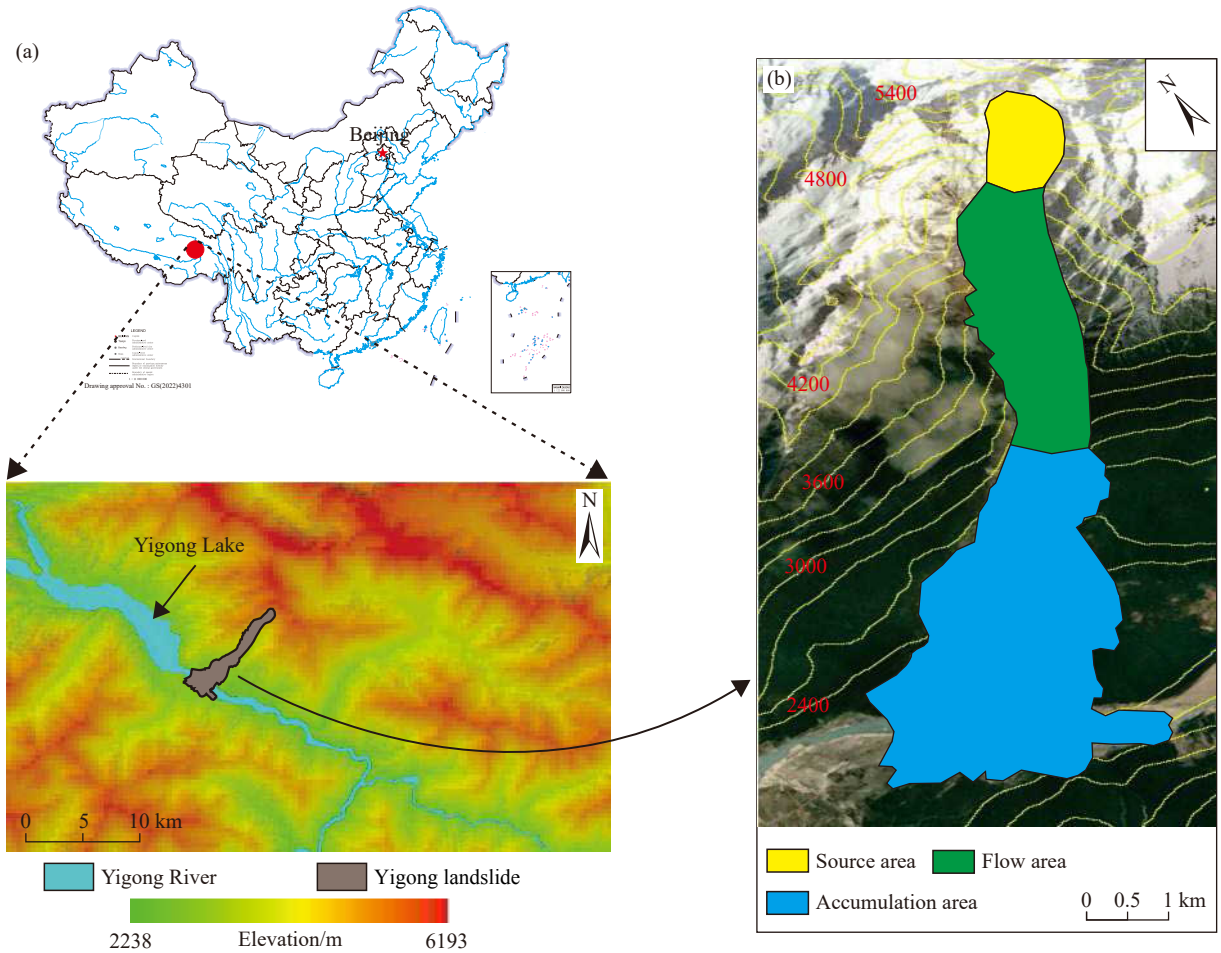

Fig. 1. a–Location of the Yigong landslide, with the 30-m DEM showing the topography around the landslide, and b– different sections of the Yigong landslide, with the contour and remote sensing image as the base map.

Yigong Township, Bomi County, Tibet of China, making it one of the largest landslides in China in nearly a century (Fig. 1). The specific location of the landslide is in the Zhamunong gully (30.178°N, 94.940°E), and the initial volume of the collapsed rock mass in the source area was approximately 9×10^7 m^3 (Xu Q et al., 2012). The landslide moved from an elevation of 5132 m to around 2163 m within 10 minutes, covering a horizontal distance of over 10 km, with an average speed of 37–39 m/s. The final deposited volume reached 3×10^8 m^3, forming a natural dam approximately 2500 m long, 2500 m wide, and with an average thickness of 60 m. This dam blocked the Yigong Zangbu River, creating a dammed lake (Delaney KB and Evans SG, 2015).

The Zhamunong gully is located on the south side of the Nyenchen Tanglha Mountains in Tibet, China, with a total length of 9.7 km and an elevation ranging from 2185 m to 5515 m, and an average slope of 31.4%. It is a northeast-southwest-oriented channel, and its mouth eventually converges into the Yigong Zangbu River Valley (Zhou J et al., 2016). The gully has a trumpet-shaped appearance on the plane, with a watershed area of 20.2 km^2. The majority of the area is covered by forests (about 10.4 km^2), followed by exposed bedrock and glacial areas (about 7.6 km^2). The mountain top is perennially covered by ice and snow, with an area of approximately 2.2 km^2 (Xu Q et al., 2012). Zhamunong gully is located at the intersection of the Jiali Fault and the Yigong-Lurang Fault, making it a typical geological structurally active zone in the Tibetan Plateau. The region mainly comprises four types of rocks: granite, marble, sandstone-shale, and limestone. The rocks are highly weathered, with well-developed joints and fractures, and their strike and slope direction are generally consistent. Under the influence of intense tectonic deformation and geomorphic evolution, geological disasters frequently occur in the region, posing significant threats to the safety of local residents and engineering activities (Cui P et al., 2022).

Yigong Township, in comparison to other regions of the Tibetan Plateau, has a lower elevation. Due to the surrounding mountain ranges, it is influenced by the warm and humid air currents from the Indian Ocean. The Yigong Zangbu River basin receives abundant rainfall, resulting in a mild climate and dense vegetation. The region has an annual average temperature of approximately 11.4°C, with an annual average precipitation of up to 960.5 mm. Additionally, there is vertical variability in precipitation in Zhamunong gully, with precipitation increasing with elevation. This phenomenon becomes more pronounced when the altitude exceeds 3500 m (Shang Y et al., 2003; Hu K et al., 2021).

2.2. Failure mechanism of the landslide

The Zhamunong gully, where the Yigong landslide is located, has been a breeding ground for large landslides. Previous studies have provided radiocarbon dating of detrital materials as evidence, confirming at least 6 occurrences of large landslide events in the past 5500 years. The most recent event took place in 1900 and also resulted in a catastrophic dam failure (Guo C et al., 2020b). From the engineering geological profile (Fig. 2), it can be observed that the area where the landslide ultimately moved corresponds to the deposit of the 1900 landslide.

For the Yigong landslide in 2000, the source area of the landslide contains massive wedge-shaped rock blocks located at the top of the Zhamunong gully, at an elevation above 5000 m, with an inclination angle of 70°–80° (Fig. 3). The study area is situated in the southeastern part of the Tibetan Plateau, one of the most tectonically active regions globally. Under the coupled influence of frequent tectonic movements, earthquakes, and geomorphic evolution, the rock mass becomes loose, and joint fractures develop well. The rock mass primarily consists of shale and granite, with shale intervals ranging from 1–5 m, and the rock mass is covered by a thick layer of ice and snow. Over an extended geological period, the shale undergoes gradual flexural deformation (Zhou J et al., 2016). Furthermore, the environment of high-altitude ice and snow coverage intensifies the freeze-thaw

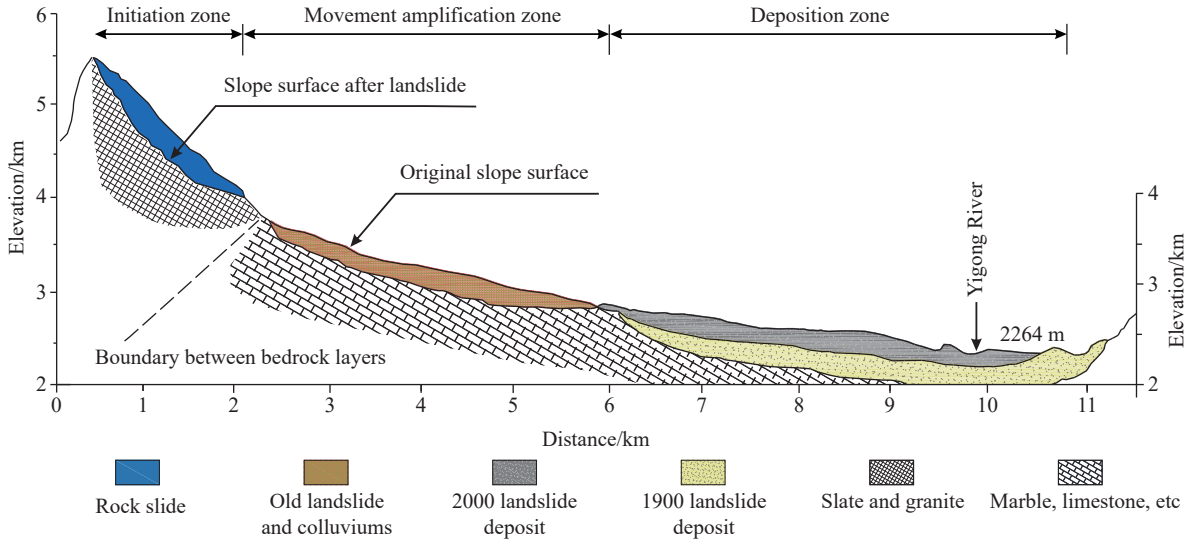

Fig. 2. Profile of the Yigong landslide showing the dynamic process of the ground surface and engineering geology characteristics.

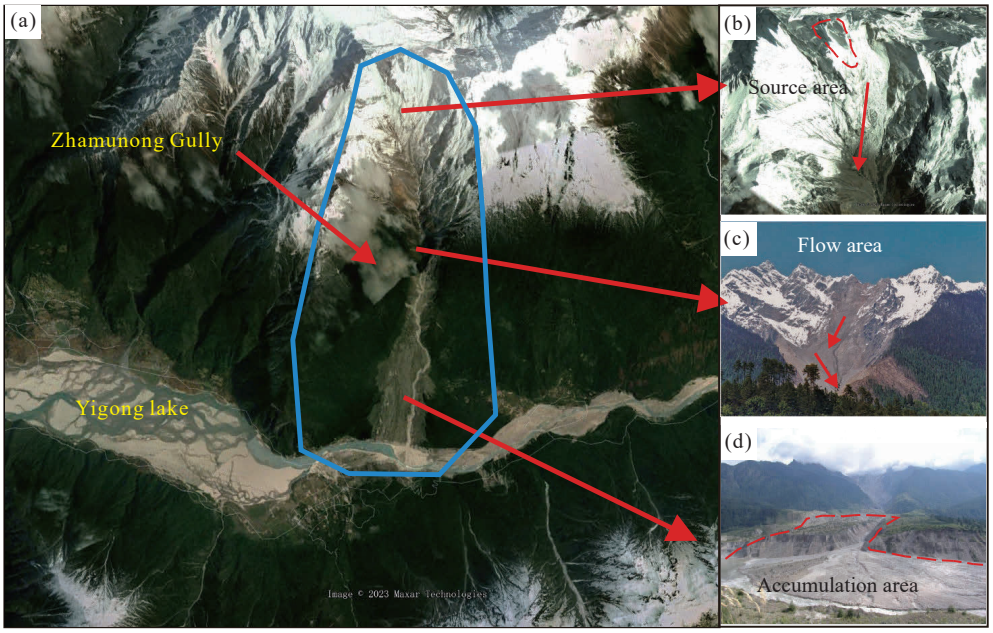

Fig. 3. Geomorphology characteristics of the Yigong landslide: (a)–overview of the Zhamunong gully and the Yigong landslide (modified from the images taken on 30 April 2006, from Google Earth), (b)–the source area covered by snow and ice at the top of the gully (modified from Delaney KB and Evans SG, 2015), (c)–the flow area, and (d) the accumulation area where the landslide dam happened (modified from Zhang M and Yin Y, 2013).

cycles in the initiation area of the landslide. On one hand, the repeated melting and freezing of ice and snow affect the aperture of structural planes and the stability of the rock mass (Huang F et al., 2023). On the other hand, the infiltration of meltwater significantly increases pore water pressure and reduces the shear strength of the rock (Crozier MJ, 2010; Guo Z et al., 2022a; Hürlimann M et al., 2022). Under these influences, the rock mass in the source area becomes noticeably loose, and there is a high risk of structural plane rupture, making it prone to high-altitude rock avalanches at any time.

From a meteorological perspective, the source area of the landslide is situated in the permafrost weathering zone, experiencing seasonal maximum temperature differences of up to 25°C. In the two months leading up to the landslide, the Zhamunong gully first underwent meteorological conditions of high temperatures and drought, followed by a transition to moderate rainfall. This indicates that the region underwent a small-scale wet-dry cycle. Specifically, the precipitation in March 2000 was significantly lower compared to the same period in previous years, but the precipitation from April 1st to 8th increased significantly (Zhou J et al., 2016). On the day of the landslide, the area had already experienced several days of high temperatures and heavy rainfall, with rainwater mixed with melted ice and snow infiltrating into the fractures of the rock mass. The water eroded the rock mass, and the resulting pore water pressure exerted compression on the rock mass, leading to the sudden failure of the wedge-shaped rock mass (Shang Y et al., 2003).

Therefore, it can be seen that the causal mechanism of the Yigong landslide is closely related to various aspects, including geological conditions, topography, freeze-thaw cycles, and precipitation. It is the result of the coupling of intrinsic geological background and exogenetic processes.

3. Methodologies

3.1. Friction weakening effect

Based on the difference in movement speed, landslides can be divided into slow-moving landslides and rapid landslides (Hungr O et al., 2014). According to rate-and-state friction laws (RSFLs), it is known that frictional forces are dependent on the sliding process and time (Spagnuolo E et al., 2016). When a landslide initiates and undergoes creep deformation (slow-moving landslides), friction gradually increases. However, when the velocity exceeds a certain threshold, the sliding speed exhibits a weakening effect (Fig. 4). Therefore, it is evident that the dynamic variation of the friction coefficient needs to be considered during the transition from creep to rapid movement in landslides, and the weakening of friction is commonly considered one of the

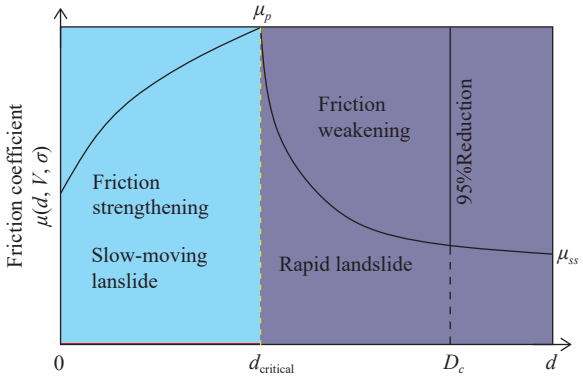

Fig. 4. Dynamic change schematic of friction in the landslides (modified from Zhang H et al. (2023)).

significant factors in the occurrence of rapid long-runout landslides (Guo Z et al., 2020c; Zhang H et al., 2023). The friction strengthening of slow-moving landslides can be investigated through rate-and-state friction equations. The object of the present study is the runout process of rapid landslide, hence the friction weakening effect is focused. In general, the frictional weakening phenomenon in rapid long-runout landslides can be explained by two categories of theories: basal friction resistance weakening and intergranular frictional resistance weakening (Yang L et al., 2023a). The former includes theories such as high-pressure steam lubrication (Goguel J, 1978), high-pressure steam lubrication (Wang F et al., 2013), and molten rock lubrication (De Blasio FV and Elverho A, 2008). The hypotheses supporting the latter category encompass acoustic fluidization (Melosh HJ, 1979), grain flow (Hsu KJ, 1975), entrainment lubrication (Dufresne A and Davies TR, 2009), and so on.

The friction coefficient of landslides is a complex parameter influenced by various factors (Fei M et al., 2012). Mizoguchi K et al. (2007) derived the friction coefficient weakening equation through high-speed rotary shear experiments on landslide materials:

$$\mu(d,V,\sigma)=\mu_{ss}(V,\sigma)+(\mu_p-\mu_{ss}(V,\sigma))\times\exp\left[\frac{\ln(0.05)\times d}{D_c}\right] \quad (1)$$

In the equation, the friction coefficient μ is considered as a variable dependent on d (shear displacement), V (shear rate), and σ (normal stress). $\mu_{ss}(V,\sigma)$ represents the residual steady-state friction coefficient affected by shear rate and normal stress. μ_p is the peak friction coefficient, and D_c is defined as the increment of shear displacement during which the friction coefficient reduces by 95% of (μ_p–μ_{ss}) from its peak value. It is evident that the friction coefficient during sliding must dynamically change. However, many studies still treat this parameter as a static value. Particularly, when conducting numerical simulations of high-velocity long-runout landslides, it is challenging to quantitatively calculate the real-time variation of the friction coefficient, leading to insufficient accuracy in the runout analysis of landslides.

3.2. Determination of the dynamic friction formula for the Yigong landslide

According to Eq (1), it can be observed that the residual steady-state friction coefficient μ_{ss} is only related to shear rate and normal stress. If only the influence of shear rate is considered, then μ_{ss} can be expressed as:

$$\mu_{ss}(V)=\mu_{ss|V=\infty}+\mu_p\times\exp(-V/V_c) \quad (2)$$

where $\mu_{ss|V=\infty}$ represents the residual steady-state friction coefficient as the shear rate tends towards infinity, and V_c is a material constant solely related to the type of soil or rock. Similarly, if only the influence of normal stress is considered, μ_{ss} can be denoted as following:

$$\mu_{ss}(\sigma)=\mu_{ss|\sigma=\infty}+\mu_p\times\exp(-\sigma/\sigma_c) \quad (3)$$

where $\mu_{ss|\sigma=\infty}$ is the residual steady-state friction coefficient as the normal stress tends towards infinity, and σ_c is likewise a material constant. Combining the two aforementioned formulas, the calculation formula for μ_{ss} can be derived as follows:

$$\mu_{ss}(V,\sigma)=\mu_{ss|V,\sigma=\infty}+\mu_p\times(\exp(-V/V_c)+\exp(-\sigma/\sigma_c)) \quad (4)$$

D_c is also related to both shear rate and normal stress, and their relationship can be expressed as:

$$D_c(V,\sigma)=iV^j+j\sigma^l \quad (5)$$

In the equation, i, j, k, and l are all material constants that may vary depending on the specific conditions of the landslide.

Hence, to obtain a dynamic friction coefficient formula for a landslide, it is necessary to determine its μ_p, μ_{ss}, D_c, and constants in the formula (V_c, σ_c, i, j, k, l). Based on detailed tests on the friction coefficient of Yigong landslide soil samples in previous studies (Wang Y et al., 2018), the peak friction coefficient of Yigong landslide soil is determined to be approximately 0.64. In the next step, a series of rotary shear tests can be conducted to obtain the steady-state friction coefficients of Yigong landslide material under two different conditions (Wang Y et al., 2017, 2018). These conditions include constant normal stress (1.47 MPa) with varying shear rates and constant shear rate (0.87 m/s) with varying normal stress. By using Eq (4) to fit the data from the two sets of tests (Fig. 5a), the quantitative functional relationships between shear rate, normal stress, and steady-state friction coefficient for the Yigong landslide can be derived as follows:

$$\mu_{ss}(V,\sigma)=0.10+0.64(\exp(-6.4V)+\exp(-1.6\sigma)) \quad (6)$$

In the equation, specific values regarding $\mu_{ss|\sigma=\infty}$, V_c and σ_c for the Yigong landslide were determined, with a corresponding correlation coefficient R^2 reaching 0.87. Subsequently, based on the peak and steady-state values of the friction coefficient, D_c was determined for different scenarios. Following that, a fitting process was applied to shear rate, normal stress, and Dc using Eq (5) (Fig. 5b), resulting in the quantitative functional relationships for the three parameters as following:

$$D_c(V,\sigma)=0.52V^{-0.84}+2.5\sigma^{-1.1} \quad (7)$$

Finally, by combining Eq (6) and (7), the formula for the dynamic friction coefficient of the Yigong landslide can be determined as following:

$$\mu=0.1+0.54\times exp\left[\frac{ln(0.05)\times d}{0.52V^{-0.84}+2.5\sigma^{-1.1}}\right] \quad (8)$$

3.3. PFC simulation

PFC is a numerical simulation tool based on the Discrete

Element Method, capable of modeling both macroscopic and microscopic features of rocks or soils. This allows the demonstration of particle material behavior under various geological and engineering scenarios (Potyondy DO and Cundall PA, 2004; Wei J et al., 2019). The software effectively simulates the deformation and flow of cohesive materials, as well as the damage and fracture processes in elastic or brittle media. Moreover, PFC's modeling capabilities are not restricted by element separation and displacement scales, enabling comprehensive simulation of the entire process from fracturing to separation in rock and soil masses, aligning with real-world scenarios of landslide initiation, movement, and disintegration (Su A et al., 2022). Hence, utilizing PFC for simulating rapid long-runout landslides offers advantages (Liu HD et al., 2018).

For this study, the specific data processing and modeling process involve several key steps. The Digital Elevation Model (DEM) data is sourced from the Shuttle Radar Topography Mission conducted by the National Aeronautics and Space Administration (NASA), with a resolution of 30 meters. This mission was carried out in February 2000, resulting in the depiction of the pre-landslide original topography. Wang Z (2006) observed a height difference in the collapsed area before and after the landslide ranging from 0 to 318 m and provided a contour map of the sliding material with a resolution of 50 m (isohyetal map). In ArcGIS, this was digitized as the sliding body section, and the sliding bed section was generated using the "Raster Calculator" tool. The ArcGIS TIFF format files were converted into STL format files recognizable by PFC3D through GlobalMapper and 3dMax software. In PFC3D, the landslide geological model was established using the sphere-wall method, which is advantageous due to its lower particle count, saving computational time. The sliding bed section was initially set as a wall, and then particles were filled within the complex enclosed surface formed by the sliding body's surface and sliding bed. The porosity was fixed at 0.3, and particle radii ranged from 10 to 20 m. The final three-dimensional geological model of the landslide was as shown in Fig. 6. It's worth noting that the volume of the top sliding body, calculated using ArcGIS, is approximately 9.3×10^7 m³, consistent with the reported values in the literature (Xu Q et al., 2012). Subsequently, particle and sliding bed calculation parameters were set based on literature (Yin Y and Xing A, 2012; Cai Z et al., 2022) and expert experience (Table 1). During the simulation process, after completing calculations for each time step, all landslide particles were retrieved, and their displacements, velocities, and normal stresses were recorded. Based on Eq (8), the friction coefficient at that moment was calculated. The new friction coefficient was compared with the previous time step, and the smaller value was selected. The simulation continued to compute the movement at the next time step until the landslide movement ceased. Additionally, it should be noted that, for ease of comparing the simulation effects of steady-state and dynamic friction, a two-dimensional model of the Yigong landslide was also established to quantitatively evaluate its sliding distance.

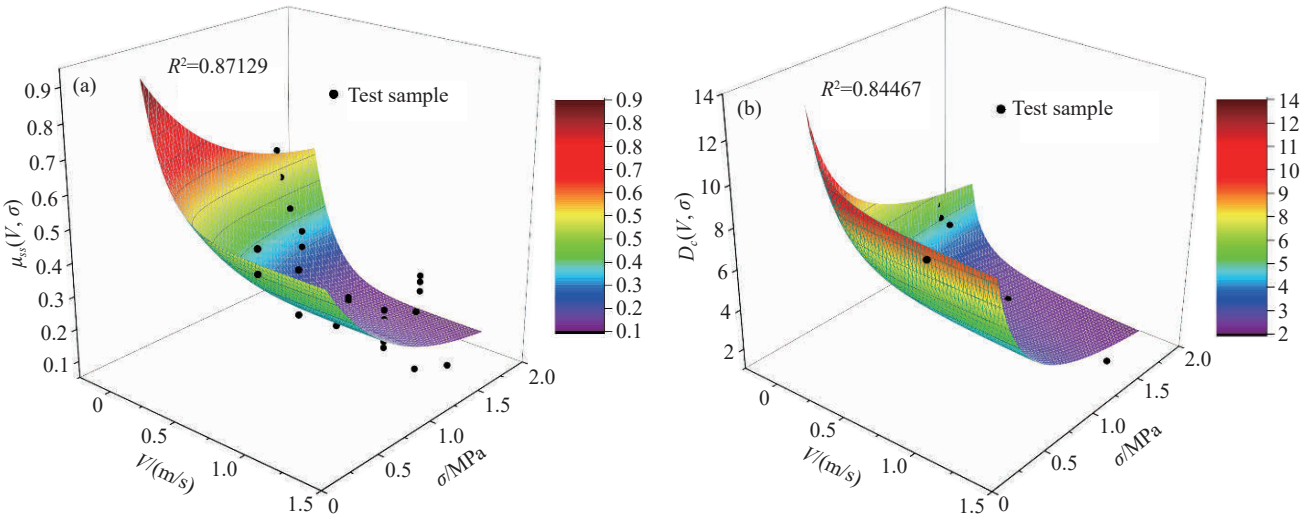

Fig. 5. (a) 3D fitting plot showing the relationship among V, σ and μ_{ss} of the Yigong landslide; (b) 3D fitting plot showing the relationship among V, σ and D_c of the Yigong landslide.

Table 1. Parameters used for the PFC3D simulation of the Yigong landslide.

Macroparameter	Density	Friction angle	cohesion	Bulk modulus	Shear modulus	Poisson's ratio
	2150 kg/m^3	38°	5 kPa	16.67 MPa	5.56 MPa	0.35
Meso-parameter	Density	Effective modulus	Normal-to-shear stiffness ratio	Cohesion of parallel bonds	Tensile strength of parallel bonds	Friction angle of parallel bonds
	2150 kg/m^3	1.0×10^8 Pa	3	5 kPa	2 kPa	38°

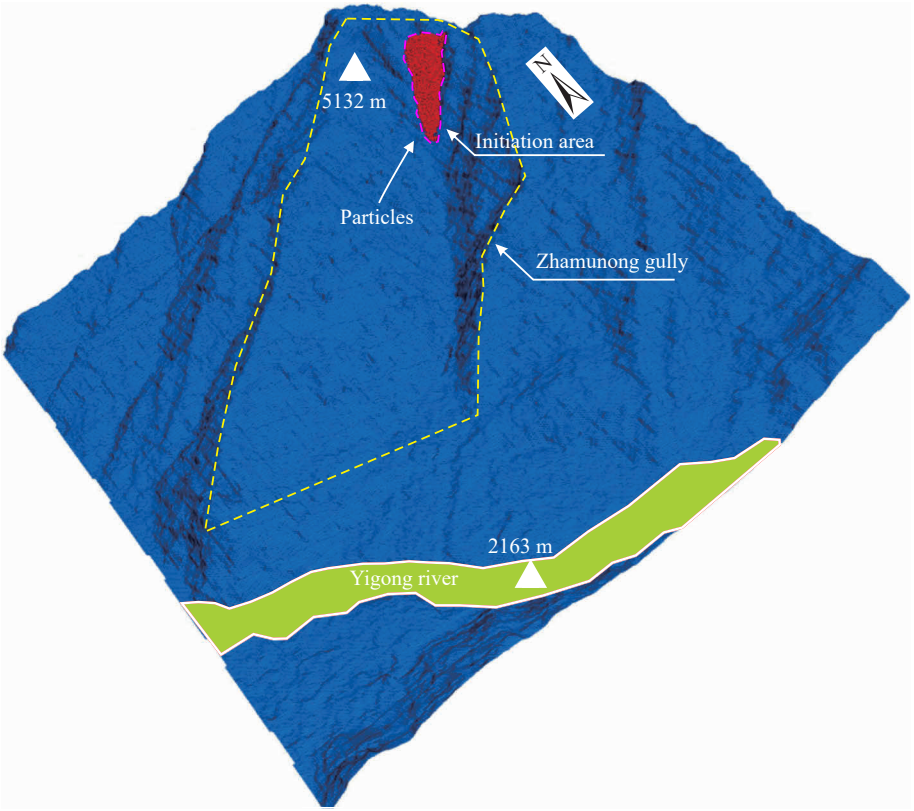

Fig. 6. 3D geological model for the Yigong landslide built in PFC3D software.

4. Results

4.1. Movement process of the Yigong landslide from the PFC simulation

Following the modeling process described in Section 3.3, PFC was used to simulate the Yigong landslide, considering the effect of friction weakening. There were totally 4955 particles generated when conducting the PFC2D simulation, whereas 17489 particles and 194502 facets for the PFC3D.

As shown in Fig. 7a, to illustrate the dynamic movement of the landslide clearly, results at different simulation times were analyzed, specifically at t=0 s, 5 s, 15 s, 30 s, 100 s, and 700 s. Within the initial 15 seconds of the landslide movement, the particles at the top of the sliding body became unstable and began moving rapidly. The minimum elevation of the sliding body swiftly changed from over 4000 m ASL to approximately 3700 m ASL. Simultaneously, the particles in the basal entrainment section moved noticeably slower. At t=30 s, the particles from the top sliding body reached the upper part of the basal entrainment zone, and collision occurred between the particles in the two sections. The basal entrainment zone began moving forward due to the impact force. However, compared to the particles at the top of the sliding body, the overall speed of the basal entrainment zone was significantly lower, as evidenced by the results at t=100 s, where most of the sliding body particles were already covering the upper part of the basal entrainment zone particles. Subsequently, the particles from both sections gradually mixed together, moved forward, and eventually came to a stop at t=700 s. The final accumulation crossed the Yigong River Valley, extending to the opposite bank, with a distance of approximately 10 km from the initial unstable position. The simulated movement time and distance align well with the reported real-world scenario.

Next, the velocity simulation results were obtained from the PFC2D (Fig. 7b). It can be see that the velocity presented similar time-dependent characteristics. During the first 30 s after the landslide initiation, the velocity gradually increased, and the peak reached 180 m/s. Meanwhile, some particles already slid to the other side of the river. However, most particles had low velocity when 100 s after the movement, and very few particles have velocities with 100 m/s. Finally, the landslide stopped at 700 s, and no particle had velocity more than 0.02 m/s at this moment.

The results regarding the three dimensional scale also supported the findings mentioned above. As seen in Fig. 8a, the locations of the particles after the sliding stopped from PFC3D simulation showed that most of them stopped within the deposit boundary. The kernel density analysis based on ArcGIS confirmed the volume of deposits was evidently larger at the bottom of the gully than the other sections. Additionally, more sliding materials flowed to the right aide due to the effect of topography (Fig. 8b). Then, a program in PFC software was coded to extract the coordinates (X, Y and H)of each ball, to create the distribution of deposit depth as Fig. 8c. It can be found that the deposit depth varied from 0 m to 120 m, and the peak value was at the bottom of the Zhamunong gully. Moreover, the depths of the center of the runout path were generally larger the edge. Although some

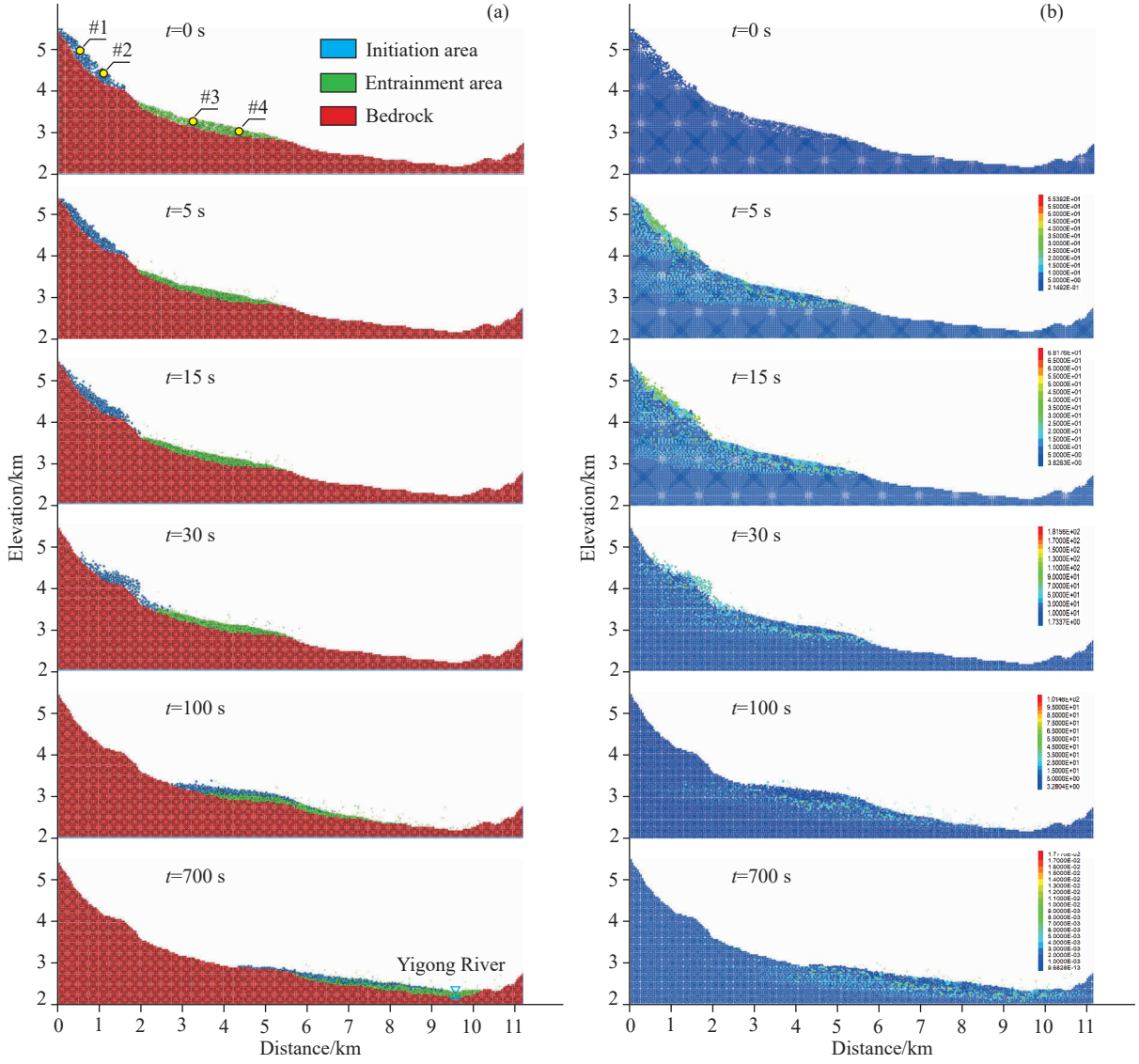

Fig. 7. (a) Simulation results from PFC2D for the Yigong landslide considering friction weakening effect at different moments, where the yellow circles show the four monitored balls #1~#4. (b) The velocity (m/s) simulation results from PFC2D for the Yigong landslide considering friction weakening effect at different moments.

uncertainties existed in the simulation results for the three dimensional scale, but overall, all the visualized results was similar with that from the existing literature, hence indicating a good accuracy of the assessment in our study.

Afterwards, four different particles were selected on the landslide to monitor changes in various indicators during their movement. Among them, #1 (h=4946 m ASL) and #2 (h=4405 m ASL) are located at the top of the sliding body, while #3 (h=3248 m ASL) and #4 (h=3008 m ASL) are in the basal entrainment zone. As seen in Fig. 9, all four monitored balls exhibit similar velocity variations: A significant initial increase in speed followed by a rapid decline, a distinct acceleration phase between t=100 s and 250 s, and then a gradual deceleration until coming to a stop. During the first acceleration phase, #1, #2, and #3 balls all reached their peak velocities around 50 s: #1 ball's speed peaked at 115.7 m/s at 42.8 s, #2 ball's maximum velocity was 132.3 m/s at 60.8 s, and #3 ball's highest speed was 32.0 m/s at 53.4 s. In contrast, #4 ball experienced its peak speed (43.6 m/s) during the first acceleration phase at 89.3 s. This is mainly because #4 is located in the lower part of the basal entrainment zone, and its motion is primarily driven by the particles above, causing a lag in velocity changes compared to the other monitored balls. Additionally, differences in velocity peak values were observed between the initiation zone and the basal entrainment zone. The former experienced a higher maximum speed during the first acceleration phase, significantly surpassing the maximum speed during the second acceleration phase. The latter exhibited smaller differences in velocity peak values between the two acceleration phases, and in some cases, the velocity during the second acceleration phase was even greater. This is primarily because the particles in the basal entrainment zone first undergo acceleration due to the pushing action of the initiation zone particles, followed by further acceleration in the later stages due to collisions and entrainment effects from the initiation zone particles. For

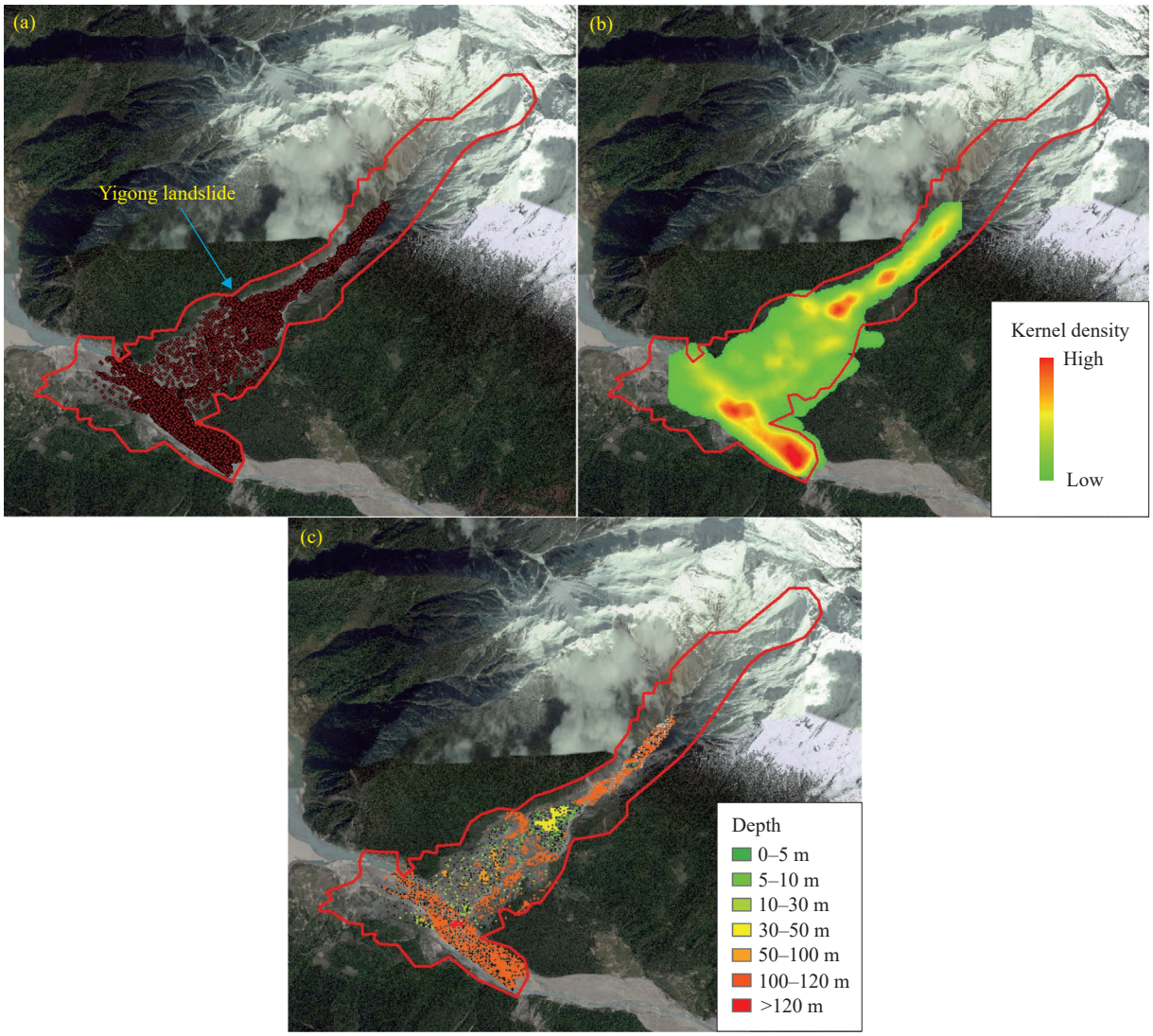

Fig. 8. 3D simulation results of the Yigong landslide, where the red line shows the boundary of the landslide deposit: (a) the positions of the particles when the simulation stopped, (b) the point density, and (c) the depth of the deposits.

initiation zone particles, the collisions between the two particle sections act as a hindrance, resulting in a smaller velocity peak in the later stages. Finally, it was noted that the maximum velocity of the monitored balls exceeded 100 m/s, consistent with descriptions in existing literature.

Overall, the simulation results regarding sliding velocity, duration and runout distance in this study fit with the actual situations of the Yigong landslide. Hence, the proposed method to consider friction weakening effect for landslide dynamic assessment is feasible.

4.2. Dynamic behavior of the friction coefficient

In addition to velocity, the characteristics of particle normal stress and displacement over time were analyzed as they are also factors influencing the friction coefficient. As seen in Fig. 10, it is evident that the rapid movement of particles in the Yigong landslide is concentrated mainly in the period from 0 to 250 s, during which the displacement contributes to over 90% of the cumulative displacement. For example, in the case of the #1 monitored ball, the displacement during the 0–250 s interval is 6890 m, while its final total displacement is 7295 m. Concerning the normal stress, its variation is characterized by two oscillation periods and a subsequent steady phase, with the amplitude of normal stress in the initiation zone particles being greater than that in the basal entrainment zone particles: the peak normal stress values for #1 and #2 monitored balls both exceed 10 MPa, while the maximum normal stress for #3 and #4 monitored balls is less than 6 MPa. It should also be noted that at certain moments, the normal stress on particles becomes zero. This occurs when the particle is not in contact or collision with other particles at that specific moment.

Despite the clear variations in particle velocity, displacement, and normal stress over time, the analysis of dynamic friction coefficient reveals that the duration of its fluctuations is very short. As seen in Fig. 11a, the duration for the four particles from the peak friction coefficient to the steady friction coefficient was 0.7 s (#1), 2.8 s (#2), 1.1 s (#3) and 0.8 s (#4), respectively. This was not a special condition but a common one, because the analysis on the average

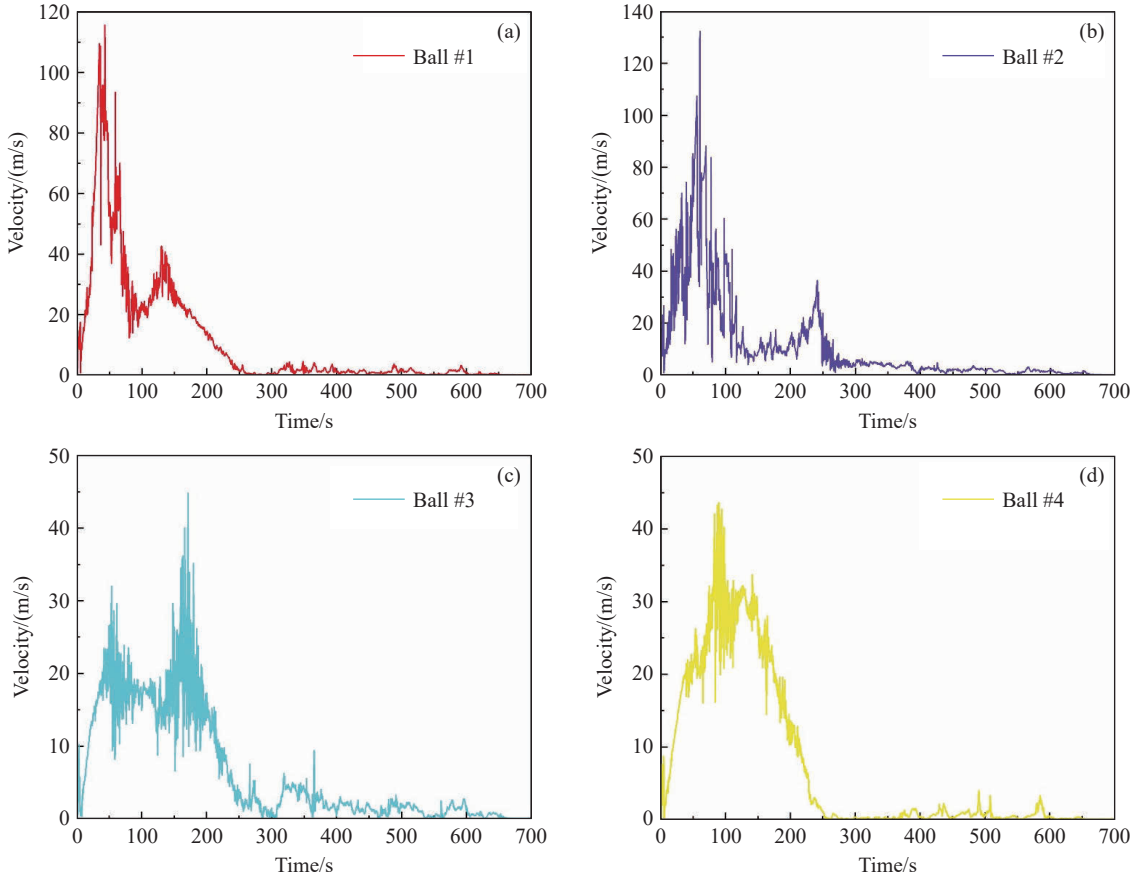

Fig. 9. Variation characteristics of velocity versus time of the four monitored balls: (a) Ball #1, (b) Ball #2, (c) Ball #3, (d) Ball #4.

friction coefficient of all the particles presented similar results (Fig. 11b). This indicated that the Yigong landslide reached the so-called "super-low friction" almost at the moment of the initiation, which provided the basis for its high velocity and long-runout distance.

4.3. Effect of friction weakening on sliding movement

Last, the numerical simulations under the scenarios with various friction coefficient were performed to verify the proposed model. Specifically, the scenarios include: (1) using the peak friction coefficient, (2) using the steady friction coefficient, and (3) using the average of the peak and steady values. All the tests applied only the static value without considering the dynamic friction law.

The simulation results are shown in Fig. 12. It can be found that the duration of the landslide movement last only 450 s when the μ was set to 0.64, and the final runout distance was approximately 7 km. This means the landslide deposits didn't cover the Yigong River in this scenario which didn't fit with the actual situation. Similar results were also observed when the friction coefficient came to the value of 0.37, under which the landslide stopped at the time of 550 s. Although the spread distance was slightly larger than the last scenario, the deposit still didn't occupy the Yigong river. When the friction coefficient was 0.1, the duration of the landslide movement last 800 s, larger than the results considering friction weakening effect. However, some particles had too high velocities during the final phase of the movement, and they exceeded the calculation area finally (for instance, μ=0.10 and t=660 s in Fig. 12). It is evident that this was unrealistic, so the simulation result under this scenario was also not reasonable, although the final runout distance was similar with that when the friction weakening effect was considered.

In one word, the results with static friction were evidently worse that that by using the proposed method, from the perspective of runout distance, movement duration or the particles behavior. This leads us to conclude that the dynamic friction seems necessary for the landslide simulation and assessment although the duration of friction weakening may be quite short.

5. Discussion

Two topics are discussed in this section: the first one is the uncertainty sources associated with the modelling procedure, where some comparisons with previous studies are also mentioned. Next, the insights that a giant landslide like Yigong landslide can provide to us are summarized.

5.1. Modelling uncertainties

In the present study, the uncertainties regarding the proposed method are mainly related to the following two aspects: (1) Friction test results of the Yigong landslide , and (2) entrainment effect. With regard to the first aspect, it

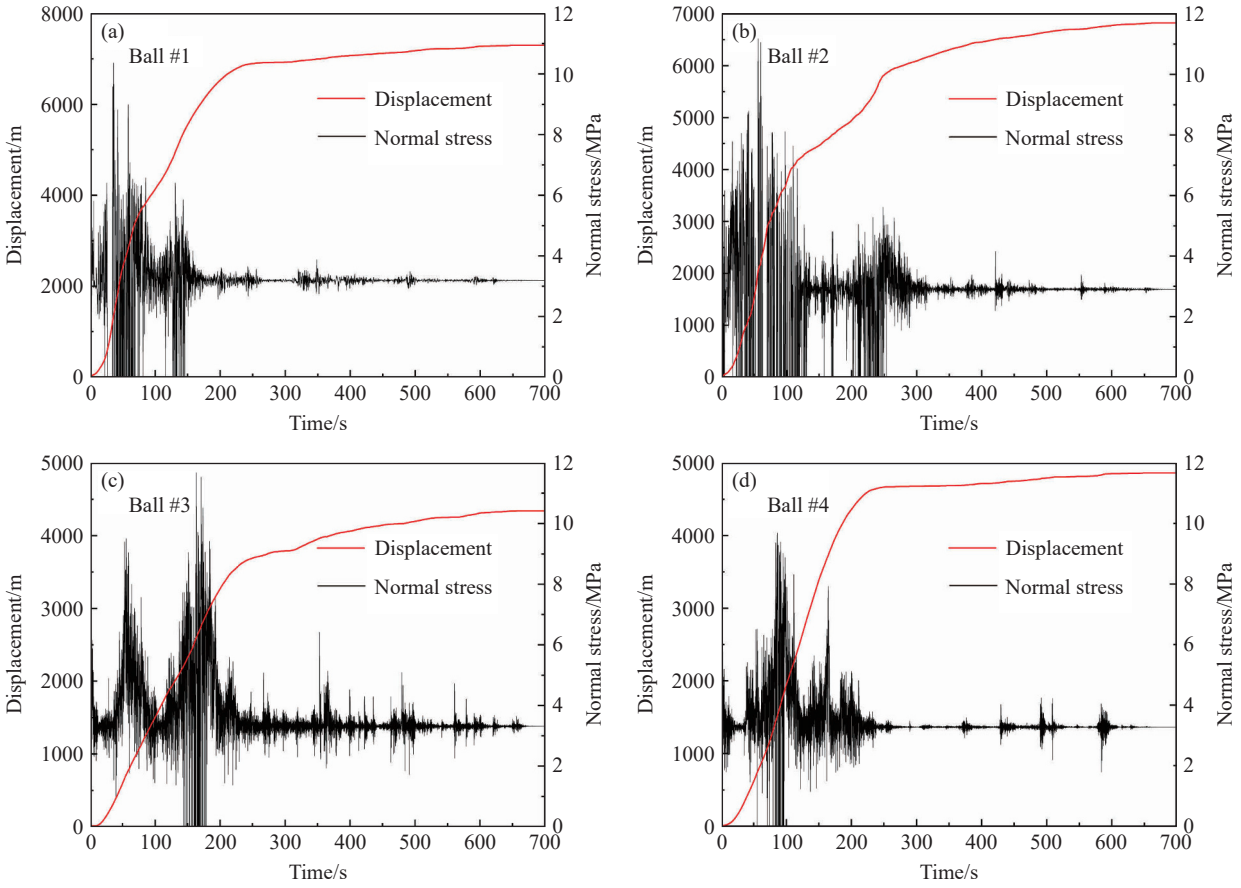

Fig. 10. Variation characteristics of displacement and normal stress versus time of the four monitored balls: (a) Ball #1, (b) Ball #2, (c) Ball #3, (d) Ball #4.

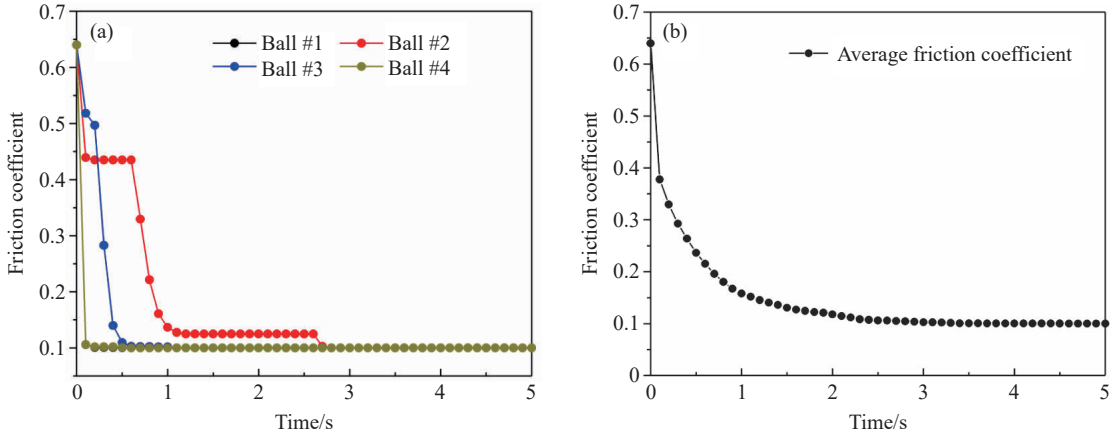

Fig. 11. (a) Values of the dynamic friction coefficient of the four monitored balls during 5 s after the landslide initiation; (b) average friction coefficient of all particles during 5 s after the landslide initiation.

should be noted that the Yigong landslide occurred in 2000, and the mechanical properties of in-suit soil samples certainly have varied with external environments. Hence, the previous studies regarding the friction test of the Yigong landslide through rotary shear test (Wang Y et al., 2017, 2018) were referred in the present study, instead of performing new laboratory test. This means the test results of peak friction coefficient as well as the relationship between friction versus normal stress and shear velocity were inherited. Additionally, Although some numerical methods (Guo C et al., 2022b; Yang L et al., 2023a) have been developed to simulate the friction weakening effect during landslide runout process, most of them were based on complex implicit solutions instead of the explicit one. Song Y et al. (2016) obtained a velocity and displacement dependent explicit friction law for Daguangbao landslide induced by Wenchuan earthquake, but normal stress was ignored. Therefore, the previous studies only involved the friction variation under single influencing factor, and our study combined the effects of three factors by deriving the explicit equation. It was more like a simplified

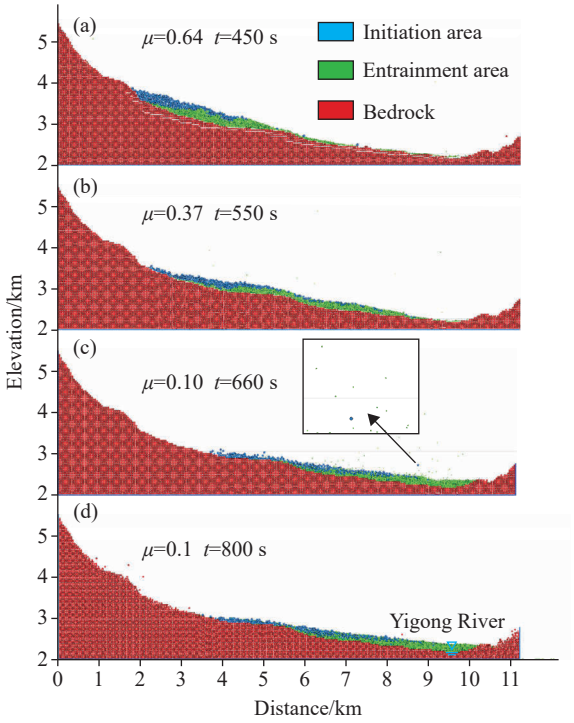

Fig. 12. Numerical simulation results under different scenarios of friction coefficient.

solution but was still considered as an improvement for this topic. The derived formula allowed to compute dynamic friction by searching the velocity, displacement and normal stress in the PFC software. Certainly, the detailed formula varies with the landslide condition and data. Hence, the shear test was necessary before the establishment of the formula suitable for a specific landslide case. Overall, the present study was more like to provide an example to show how to achieves this procedure, and the simulation result indeed confirmed that the dynamic assessment of the landslide runout was improved when the friction variation was considered.

The second uncertainty source was associated with the entrainment effect during the landslide movement process. It is well known material entrainment can significantly magnify landslide volume and increase its destructive power (Shen P et al., 2020). The experience on the Yigong landslide also supported this point: the final deposits had an almost three times bigger than the initial volume (Shang Y et al., 2003; Xu Q et al., 2012). However, the simulation for entrainment effect based on discrete element method (DEM) is always an operational challenge for engineering geologies, which is mainly subject to its theoretical basis. If the ball- ball contact method was utilized to build the landslide model, the discretization of the sliding bed material was quite time consuming given the scale of the Yigong landslide. In fact, the construction of a totally discretized 3D model for the Yigong landslide was indeed tried in this study, and the duration for model establishment and dynamic solution for friction last over three days. Herein, a totally discretized model means the discretization of both sliding mas and sliding bed. All the calculations were performed by a computer with one 8-cores 1.8 GHz CPU and 8 GB of RAM, and the simulation stopped with a convergence condition less than 10^4. Hence, our computation finally applied the wall-ball contact method to obtain the 3D model to balance the computational efficiency and accuracy. Similarly, many previous studies (Guo C et al., 2022b; Yang L et al., 2023a) also ignored the modelling for sliding bed when using the DEM methods, which means it failed to simulate the entrainment effect. However, it should be mentioned that the entrainment effect was still achieved in the 2D profile of the landslide in this study, which was evidently different from the studies mentioned above. The materials in the entrainment area was separately modelled from the sliding bed, and the results showed the good assessment accuracy. Last but not least, some techniques and tools that can consider the basal entrainment have been developed and proposed, including DAN-3D, Iverson-Ouyang model (Iverson RM and Ouyang C, 2015), MatDEM (Song D and Du H, 2023) etc. Hence, how to incorporate the friction weakening and entrainment effects together may be of high interest in the future.

5.2. Lessons from the Yigong landslide

Recently, several giant landslides were reported worldwide especially in the Tibetan Plateau, and have caused massive losses. This makes many scientists begin to look back and examine the Yigong landslide occurring 20 years ago. From the perspective of geological backgrounds, it is evident that the Yigong landslide is almost inevitable (Shang Y et al., 2003). However, its catastrophic consequences was accidental and related with more aspects. First, the rock failure had huge gravitational potential energy initially due to high elevation, and narrow gully provided good condition for mass movement. Next, the geohazard chain occurred due to the sliding mass spread to the Yigong Lake to cause the landslide dam and subsequent dam-failure. This is a similar case also happened to the Chamoli landslide in India recently, which caused more than 200 deaths due to the flood induced by the landslide dam destroyed the villages nearby (Qi W et al., 2021). It can be found that topography, geomorphology, and even number of elements at risk are all the factor that affect the consequence of a landslide event. This condition made us to conclude that the settlements downstream of the alpine inland lake may be post by high landslide and flood risk. Hence, no matter the simulation result is, the lessons from this kind of rapid long-runout landslides must be paid attention. In particular, some large-scale engineering projects are being constructed in the Tibetan Plateau, for instance the well-known Sichuan-Tibet Railway (Cui P et al., 2022). It is predictable that more geohazards will be induced by human activities combined with climate change in the area (Agterberg F, 2022; Yang G et al., 2023b; Guo Z et al., 2024). However, proactive engineering measures including anti-slide pile is difficult to implement in the alpine settings, hence the protective alternatives may be better options to reduce landslide risk, but their benefits must be analyzed and

discussed.

6. Conclusions

(i) The dynamic simulation of rapid long-runout landslides seldom consider the impact of friction weakening. Regarding this issue, this study proposed a novel method to quantify the dynamic friction law during the landslide movement. The derived friction formula was an explicit solution dependent om velocity, displacement and normal stress obtained from the rotary shear test.

(ii) The simulation of the dynamic friction law based on PFC in the case of the Yigong landslide in the Tibetan Plateau of China showed good performances: the overall movement process last about 10 minutes with the max velocity more than 120 m/s, and the spread distance approximately 10 km. All these kinematic indicators fit well with the actual situation. The variation of the average friction coefficient of the particles showed the friction decreased to the steady value from the peak value only 5 s after the sliding initiation. This indicated that the Yigong landslide reached the so-called "super-low friction" almost at the moment of the initiation.

(iii) Evident differences regarding the landslide movement were observed when it came to a comparison between the simulation results regarding dynamic friction and static friction. This demonstrated although the duration of the friction weakening effect was quite short, it was probably necessary for assessment of rapid landslides.

CRediT authorship contribution statement

Zi-zheng Guo, Xin-yong Zhou, Da Huang and Shi-jie Zhai conceived of the presented idea. Shi-jie Zhai, Bi-xia Tian and Guang-ming Li carried out the experiment and simulation. All authors discussed the results and contributed to the final manuscript.

Declaration of competing interest

The authors declare no conflicts of interest.

Acknowledgement

This research is funded by the National Natural Science Foundation of China (42307248, U23A2047, and 42277187), Natural Science Foundation of Hebei Province (D2022202005), and Planning and Natural Resources Research Project of Tianjin City (2022-40, KJ[2024]25). Bi-xia Tian wants to thank the support from the Graduated Student Innovation Funding Project of Hebei Province (CXZZSS2024007).

References

Agterberg F. 2022. How can earth science help reduce the adverse effects of climate change? Journal of Earth Science, 33 (5), 1338–1338. doi:10.1007/s12583-022-1741-y

Cai Z, Liu E, Chen N, Feng J, Hu G, Su Y. 2022. Numerical analysis of the initiation and sliding process of the Yigong landslide using a continuous–discontinuous method. Environmental Earth Sciences, 81(5), 150. doi: 10.1007/s12665-022-10279-y.

Crozier MJ. 2010. Deciphering the effect of climate change on landslide activity: A review. Geomorphology, 124(3–4), 260–267. doi: 10.1016/j.geomorph.2010.04.009.

Cui P, Ge Y, Li S, Li Z, Xu X, Zhou GGD, Chen H, Wang H, Lei Y, Zhou L, Yi S, Wu C, Guo J, Wang Q, Lan H, Ding M, Ren J, Zeng L, Jiang Y, Wang Y. 2022. Scientific challenges in disaster risk reduction for the Sichuan–Tibet Railway. Engineering Geology, 309, 106837. doi:10.1016/j.enggeo.2022.106837

Dawso AG, Matthews JA, Shakes RA. 2017. A catastrophic landslide (Sturzstrom) in Verkilsdalen, Rondane National Park, Southern Norway. Physical Geography, 68(1–2), 77–87. doi: 10.1080/04353676.1986.11880160.

De Blasio FV, Elverho A. 2008. A model for frictional melt production beneath large rock avalanches. Journal of Geophysical Research: Earth Surface, 113, F02014. doi: 10.1029/2007JF000867.

Delaney KB, Evans SG. 2015. The 2000 Yigong landslide (Tibetan Plateau), rockslide-dammed lake and outburst flood: Review, remote sensing analysis, and process modelling. Geomorphology, 246, 377–393. doi: 10.1016/j.geomorph.2015.06.020.

Dufresne A, Davies TR. 2009. Longitudinal ridges in mass movement deposits. Geomorphology, 105(3–4), 171–181. doi: 10.1016/j.geomorph.2008.09.009.

Fei M, Sun Q, Zhong D, Zhou GG. 2012. Simulations of granular flow along an inclined plane using the Savage–Hutter model. Particuology, 10(2), 236–241. doi: 10.1016/j.partic.2011.11.007.

Feng ZY, Lo CM, Lin QF. 2017. The characteristics of the seismic signals induced by landslides using a coupling of discrete element and finite difference methods. Landslides, 14, 661–674. doi: 10.1007/s10346-016-0714-6.

Fort M. 2000. Glaciers and mass wasting processes: Their influence on the shaping of the Kali Gandaki valley (higher Himalaya of Nepal). Quaternary International, 65–66, 101–119. doi:10.1016/S1040-6182(99)00039-7

Goguel J. 1978. Chapter 20 - Scale-Dependent Rockslide Mechanisms, with Emphasis on the Role of Pore Fluid Vaporization. Rockslides and Avalanches, 14, 693–705.

Guo Z, Chen L, Yin K, Shrestha DP, Zhang L. 2020a. Quantitative risk assessment of slow-moving landslides from the viewpoint of decision-making: A case study of the Three Gorges Reservoir in China. Engineering Geology, 273, 105667. doi: 10.1016/j.enggeo.2020.105667.

Guo C, Montgomery DR, Zhang Y, Zhong N, Fan C, Wu R, Yang Z, Ding Y, Jin J, Yan Y. 2020b. Evidence for repeated failure of the giant Yigong landslide on the edge of the Tibetan Plateau. Scientific Reports, 10, 14371. doi: 10.1038/s41598-020-71335-w.

Guo Z, Chen L, Gui L, Du J, Yin K, Do HM. 2020c. Landslide displacement prediction based on variational mode decomposition and WA-GWO-BP model. Landslides, 17, 567–583. doi: 10.1007/s10346-019-01314-4.

Guo Z, Torra O, Hürlimann M, Medina V, Puig-Polo C. 2022a. FSLAM: A QGIS plugin for fast regional susceptibility assessment of rainfall-induced landslides. Environmental Modelling and Software, 150, 105354. doi: 10.1016/j.envsoft.2022.105354.

Guo J, Cui Y, Xu W, Shen W, Li T, Yi S. 2022b. A novel friction weakening-based dynamic model for landslide runout assessment along the Sichuan-Tibet Railway. Engineering Geology, 306, 106721. doi: 10.1016/j.enggeo.2022.106721.

Guo Z, Tian B, He J, Xu C, Zeng T, Zhu Y. 2023. Hazard assessment for regional typhoon-triggered landslides by using physically-based model -A case study from southeastern China. Georisk: Assessment and Management of Risk for Engineered Systems and Geohazards,

17(4), 740–754. doi: 10.1080/17499518.2023.2188465.
Guo Z, Tian B, Zhu Y, He J, Zhang T. 2024. How do the landslide and non-landslide sampling strategies impact landslide susceptibility assessment? — A case study at catchment scale from China. Journal of Rock Mechanics and Geotechnical Engineering, 16(3), 877–894. doi: 10.1016/j.jrmge.2023.07.026.
Hsu K J. 1975. Catastrophic debris streams (sturzstroms) generated by rockfalls. Geological Society of America Bulletin, 86(1), 129–140. doi: 10.1130/0016-7606(1975)86<129:CDSSGB>2.0.CO;2.
Hu K, Wu C, Wei L, Zhang X, Zhang Q, Liu W, Yanites BJ. 2021. Geomorphic effects of recurrent outburst superfloods in the Yigong River on the southeastern margin of Tibet. Scientific Reports, 11(1), 15577. doi: 10.1038/s41598-021-95194-1.
Huang T, Ding M, She T, Tian S, Yang J. 2017. Numerical simulation of a high-speed landslide in Chenjiaba, Beichuan, China. Engineering Geology, 14(11), 2137–2149. doi: 10.1007/s11629-017-4516-7.
Huang F, Xiong H, Chen S, Lv Z, Huang J, Chang Z, Catani F. 2023. Slope stability prediction based on a long short-term memory neural network: Comparisons with convolutional neural networks, support vector machines and random forest models. International Journal of Coal Science and Technology, 10(1), 18. doi: 10.1007/s40789-023-00579-4.
Hungr O, Leroueil S, Picarelli L. 2014. The Varnes classification of landslide types, an update. Landslides, 11(2), 167–194. doi: 10.1007/s10346-013-0436-y.
Hürlimann M, Guo Z, Puig-Polo C, Medina V. 2022. Impacts of future climate and land cover changes on landslide susceptibility: regional scale modelling in the Val d'Aran region (Pyrenees, Spain). Landslides, 19(1), 99–118. doi: 10.1007/s10346-021-01775-6.
Iverson RM, Ouyang C. 2015. Entrainment of bed material by Earth-surface mass flows: Review and reformulation of depth-integrated theory. Reviews of Geophysics, 53(1), 27–58. doi: 10.1002/2013RG000447.
Jaboyedoff M, Oppikofer T, Abellán A, Derron MH, Loye A, Metzger R, Pedrazzini A. 2012. Use of LIDAR in landslide investigations: a review. Natural hazards, 61, 5–28. doi: 10.1007/s11069-010-9634-2.
Lin A, Ren Z, Kumahara Y. 2010. Structural analysis of the coseismic shear zone of the 2008 Mw 7.9 Wenchuan earthquake, China. Journal of Structural Geology, 32 (6), 781–791. doi:10.1016/j.jsg.2010.05.004
Liu HD, Li DD, Wang ZF. 2018. Dynamic process of the Wenjiagou rock landslide in Sichuan Province, China. Arabian Journal of Geosciences, 11, 1–19. doi: 10.1007/s12517-018-3564-9.
Liu W, He S. 2018. Dynamic simulation of a mountain disaster chain: Landslides, barrier lakes, and outburst floods. Natural Hazards, 90, 757–775. doi: 10.1007/s11069-017-3073-2.
Liu W, He S, Li X, Xu Q. 2016. Two-dimensional landslide dynamic simulation based on a velocity-weakening friction law. Landslides, 13, 957–965. doi: 10.1007/s10346-015-0632-z.
Luo J, Pei X, Evans SG, Huang R. 2019. Mechanics of the earthquake-induced Hongshiyan landslide in the 2014 Mw 6.2 Ludian earthquake, Yunnan, China. Engineering Geology, 251, 197–213. doi:10.1016/j.enggeo.2018.11.011
Ma P, Peng J, Zhuang J, Zhu X, Liu C, Cheng Y, Zhang Z. 2022. Initiation Mechanism of Loess Mudflows by Flume Experiments. Journal of Earth Science, 33(5), 1166–1178. doi: 10.1007/s12583-022-1660-y.
Melosh HJ. 1979. Acoustic fluidization: A new geologic process? Journal of Geophysical Research: Solid Earth, 84 (B13), 7513–7520. doi:10.1029/JB084iB13p07513
Mizoguchi K, Hirose T, Shimamoto T, Fukuyama E. 2007. Reconstruction of seismic faulting by high-velocity friction experiments: An example of the 1995 Kobe earthquake. Geophysical Research Letters, 34(1), L01038. doi: 10.1029/2006GL027931.
Moore DE, Lockner, DA. 2008. Talc friction in the temperature range 25–400 C: Relevance for fault-zone weakening. Tectonophysics, 449(1-4), 120–132. doi: 10.1016/j.tecto.2007.11.039.
Ouyang C, Zhao W, He S, Wang D, Zhou S, An H, Wang Z, Cheng D. 2017. Numerical modeling and dynamic analysis of the 2017 Xinmo landslide in Maoxian County, China. Journal of Mountain Science, 14, 1701–1711. doi: 10.1007/s11629-017-4613-7.
Pritchard MA, Savigny K. 1991. The Heather Hill landslide: An example of a large scale toppling failure in a natural slope. Canadian Geotechnical Journal, 28(3), 410–422. doi: 10.1139/t91-051.
Potyondy DO, Cundall PA. 2004. A bonded-particle model for rock. International journal of rock mechanics and mining sciences, 41(8), 1329–1364. doi: 10.1016/j.ijrmms.2004.09.011.
Qi W, Yang W, He X, Xu C. 2021. Detecting Chamoli landslide precursors in the southern Himalayas using remote sensing data. Landslides, 18, 3449–3456. doi: 10.1007/s10346-021-01753-y.
Royden LH, Burchfiel BC, Van Der Hilst R. 2008. The geological evolution of the Tibetan Plateau. Science, 321(5892), 1054–1058. doi: 10.1126/science.115537.
Schneider D, Huggei C, Haeberli W, Kaitna R. 2011. Unraveling driving factors for large rock–ice avalanche mobility. Earth Surface Processes and Landforms, 36(14), 1948–1966. doi: 10.1002/esp.2218.
Shang Y, Yang Z, Li L, Liao Q, Wang Y. 2003. A super-large landslide in Tibet in 2000: Background, occurrence, disaster, and origin. Geomorphology, 54(3–4), 225–243. doi: 10.1016/S0169-555X(02)00358-6.
Shen P, Zhang L, Wong H, Deng D, Zhou S, Zhang S, Chen C. 2020. Debris flow enlargement from entrainment: A case study for comparison of three entrainment models. Engineering Geology. 270, 105581. doi:10.1016/j.enggeo.2020.105581
Song Y, Huang D, Ce D. 2016. Numerical modelling of the 2008 Wenchuan earthquake-triggered Daguangbao landslide using a velocity and displacement dependent friction law. Engineering Geology, 215, 50–68. doi: 10.1016/j.enggeo.2016.11.003.
Song D, Du H. 2023. Numerical investigation of the evolution process of an open-pit mine landslide using discrete-element method. International Journal of Geomechanics, 23(6), 7568. doi: 10.1061/IJGNAI.GMENG-7568.
Spagnuolo E, Nielsen S, Violay M, Di Toro G. 2016. An empirically based steady state friction law and implications for fault stability. Geophysical Research Letters, 43(7), 3263–3271. doi: 10.1002/2016GL067881.
Su A, Feng M, Dong S, Zou Z, Wang J. 2022. Improved statically solvable slice method for slope stability analysis. Journal of Earth Science, 33(5), 1190–1203. doi: 10.1007/s12583-022-1631-3.
Wang F, Sun P, Highland L, Cheng Q. 2013. Initiation and motion mechanism of the Donghekou rapid and long runout landslide triggered by the 2008 Wenchuan earthquake, China. Earthquake-Induced Landslides, 473–483. doi:10.1007/978-3-642-32238-9_50
Wang W, Chen G, Zhang H, Zhou S, Liu S, Wu Y Q, Fan F. 2016. Analysis of landslide-generated impulsive waves using a coupled DDA-SPH method. Engineering Analysis with Boundary Elements, 64, 267–277. doi: 10.1016/j.enganabound.2015.12.014.
Wang Y, Dong J, Cheng Q. 2017. Velocitdepey-ndent frictional weakening of large rock avalanche basal facies: Implications for rock avalanche hypermobility? Journal of Geophysical Research: Solid Earth, 122 (3), 1648–1676. doi:10.1002/2016JB013624
Wang Y, Dong J, Cheng Q. 2018. Normal stress-dependent frictional weakening of large rock avalanche basal facies: Implications for the rock avalanche volume effect. Journal of Geophysical Research:Solid Earth, 123(4), 3270–3282. doi: 10.1002/2018JB015602.
Wang Z. 2006. Large scale individual landslide remote sensing. Earth Science Frontiers, 13(5), 516 (in Chinese with English).

Wei J, Zhao Z, Xu C, Wen Q. 2019. Numerical investigation of landslide kinetics for the recent Mabian landslide (Sichuan, China). Landslides, 16, 2287–2298. doi: 10.1007/s10346-019-01237-0.

Wu JH, Lin W, Hu H. 2018. Post-failure simulations of a large slope failure using 3DEC: The Hsien-du-shan slope. Engineering Geology, 242, 92–107. doi: 10.1016/j.enggeo.2018.05.018.

Xing A, Wang G, Li B, Jiang Y, Feng Z, Kamai T. 2015. Long-runout mechanism and landsliding behaviour of large catastrophic landslide triggered by heavy rainfall in Guanling, Guizhou, China. Canadian Geotechnical Journal, 52(7), 971–981. doi: 10.1139/cgj-2014-0122.

Xu Q, Shang Y, Asch van T, Wang S, Zhang Z, Dong X. 2012. Observations from the large, rapid Yigong rock slide–debris avalanche, southeast Tibet. Canadian Geotechnical Journal, 49(5), 589–606. doi: 10.1139/t2012-021.

Yang L, Zhang M, Jiao W, Wu Y, Zhang C, Wang Z. 2023a. Influence of intergranular friction weakening on rock avalanche dynamics. Computers and Geotechnics, 159, 105440. doi: 10.1016/j.compgeo.2023.105440.

Yang G, Chen Y, Liu X, Yang Ri, Zhang Y, Zhang J. 2023b. Stability analysis of a slope containing water-sensitive mudstone considering different rainfall conditions at an open-pit mine. International Journal of Coal Science and Technology, 10(1), 64. doi: 10.1007/s40789-023-00619-z.

Yin Y, Xing A. 2012. Aerodynamic modeling of the Yigong gigantic rock slide-debris avalanche, Tibet, China. Bulletin of Engineering Geology and the Environment, 71, 149–160. doi: 10.1007/s10064-011-0348-9.

Zhang H, He S, Liu W, Deng Y, Hu W. 2023. Creep-to-runout transition of large landslides controlled by frictional velocity strengthening and weakening (Vajont 1963, Italy). Rock Mechanics and Rock Engineering, 56, 8471–8483. doi: 10.1007/s00603-023-03473-2.

Zhang Z, Wang T, Wu S, Tang H, Liang C. 2017. The role of seismic triggering in a deep-seated mudstone landslide, China: Historical reconstruction and mechanism analysis. Engineering Geology, 226, 122–135. doi: 10.1016/j.enggeo.2017.06.001.

Zhang M, Yin Y. 2013. Dynamics, mobility-controlling factors and transport mechanisms of rapid long-runout rock avalanches in China. Engineering Geology, 167, 37–58. doi: 10.1016/j.enggeo.2013.10.010.

Zhao N, Zhang R, Yan E, He X, Liu J. 2020. A dynamic model for rapid startup of high-speed landslides based on the mechanism of friction-induced thermal pressurization considering vaporization. Landslides, 17, 1545–1560. doi: 10.1007/s10346-020-01372-z.

Zhao T, Dai F, Xu N. 2017. Coupled DEM-CFD investigation on the formation of landslide dams in narrow rivers. Landslides, 14, 189–201. doi: 10.1007/s10346-015-0675-1.

Zhou J, Cui P, Hao M. 2016. Comprehensive analyses of the initiation and entrainment processes of the 2000 Yigong catastrophic landslide in Tibet, China. Landslides, 13, 39–54. doi: 10.1007/s10346-014-0553-2.

Zhu C, Huang Y, Zhan L. 2018. SPH-based simulation of flow process of a landslide at Hongao landfill in China. Natural Hazards, 93, 1113–1126. doi: 10.1007/s11069-018-3342-8.